Analytica Chimica Acta 1368 (2025) 344331

Contents lists available at ScienceDirect

Analytica Chimica Acta

journal homepage: www.elsevier.com/locate/aca

Dual-strain detection of norovirus GI.1 and GII.4 in food samples using epitope-imprinted polymers

Amy Dann [a,b], Pankaj Singla [a], Jake McClements [b], Minji Kim [c], Sloane Stoufer [c], Robert D. Crapnell [d], Craig E. Banks [d], Shayan Seyedin [b], Mark Geoghegan [b], Christopher F. Blanford [e,f], Matthew D. Moore [c,*], Marloes Peeters [a,**]

[a] Department of Chemical Engineering, University of Manchester, Nancy Rothwell Building, East Both Street, Manchester, M13 9QS, Great Britain
[b] School of Engineering, Newcastle University, Claremont Road, Newcastle-Upon-Tyne, NE1 7RU, United Kingdom
[c] Department of Food Science, University of Massachusetts, Amherst, MA, 01003, United States
[d] Faculty of Science and Engineering, Manchester Metropolitan University, Dalton Building, Chester Steet, Manchester, M1 5GD, UK, Great Britain
[e] Manchester Institute of Biotechnology, The University of Manchester, 131 Princess Street, Manchester, M1 7DN, United Kingdom
[f] Department of Materials, School of Natural Sciences, University of Manchester, Oxford Road, M13 9PL, Great Britain

HIGHLIGHTS

- Dual norovirus strain recognition for rapid, on-site detection in food matrices.
- Epitope imprinted nanoMIPs integrated into cost-effective thermal sensor.
- 30-min detection time in high-risk food samples for outbreak prevention.
- Selectivity exploration using human norovirus surrogates.

GRAPHICAL ABSTRACT

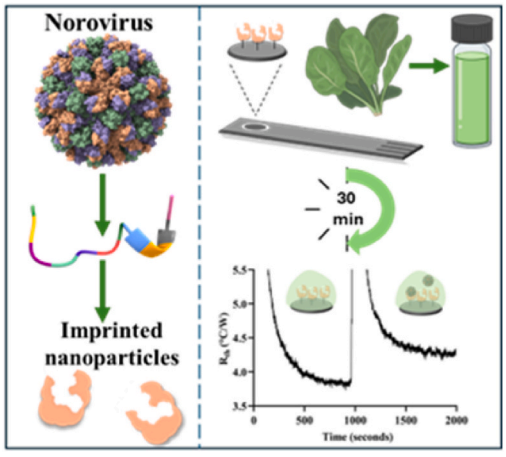

ARTICLE INFO

Keywords:
Molecularly imprinted polymers (MIP)
Biomimetic sensor
Foodborne illness
Epitope imprinting

ABSTRACT

Background: Norovirus is the leading cause of viral gastroenteritis worldwide, contributing to widespread disease and financial burdens. However, current testing methods are unsuitable for on-site analysis, as they typically use biological receptors, require specialized reagents, and skilled technicians. Proactive on-site testing of high-risk food samples is essential to prevent outbreaks, requiring the development of innovative sensor systems.
Results: We have developed a thermal sensor capable of selectively detecting two recurrent norovirus genotypes, GI.1 and GII.4, within a model food matrix. The sensor uses epitope-imprinted polymer nanoparticles (nanoMIPs)

* Corresponding author.
** Corresponding author.
E-mail address: marloes.peeters@manchester.ac.uk (M. Peeters).

https://doi.org/10.1016/j.aca.2025.344331
Received 11 March 2025; Received in revised form 11 June 2025; Accepted 12 June 2025
Available online 12 June 2025

Norovirus
Heat transfer method (HTM)

designed from a 10-amino-acid sequence derived from the conserved P1 region of the GI.1 viral capsid. The nanoMIPs demonstrated favorable detection capability to norovirus GI.1 and GII.4 virus-like particles in buffer solutions, achieving detection limits of 1.53 and 2.28 pg/mL, respectively. The selectivity of the nanoMIPs was evaluated against a panel of similar viruses, including murine norovirus, Tulane virus, and bacteriophage MS2, each of which showed a reduced signal. Notably, the sensor achieved rapid detection (30 min) of norovirus GI.1 and GII.4 virus-like particles in contamination prone spinach samples while maintaining comparable detection limits (2.19 pg/mL and 2.69 pg/mL) to spiked buffer solutions.

Significance: The combination of rapid detection time, dual strain recognition, and simple sample preparation makes this thermal sensor a promising tool for on-site testing in food safety and public health settings. Furthermore, the ability to detect multiple strains using a single ligand represents a significant advantage, enabling the development of straightforward systems capable of detecting various strains in complex environments.

1. Introduction

The advancement of molecular technologies for straightforward and cost-effective diagnostics has emerged as a key priority in the field of biotechnology [1]. Additionally, the rise of point-of-care testing has become an invaluable tool for proactive disease prevention [2]. The need for these testing devices is particularly crucial in lower-income areas, where diarrheal diseases significantly contribute to high mortality rates [3]. Norovirus is the leading cause of foodborne gastroenteritis worldwide causing 5.5 million cases of foodborne illness annually in the United States alone [4,5]. In developing countries, norovirus is estimated to cause approximately 200,000 deaths each year, with around 70,000 of those being children [6]. A longitudinal study conducted across eight developing countries reported that 89 % of children experienced at least one norovirus infection by age two, highlighting the prevalence of infections in early childhood [7]. Efforts to prevent norovirus have grown, with significant progress toward a viable vaccine [8]. Such a vaccine could shift attention to preventive strategies that reduce the severe outbreaks frequently seen in healthcare settings, schools, and other high-contact environments. While a vaccine has the potential to significantly reduce norovirus cases, it is still under development, and its global distribution may face limitations. As a result, proactive testing of food samples remains crucial to manage outbreaks effectively.

First identified in the early 1970s, norovirus is an enteric virus composed of positive-sense single-stranded RNA and is part of the *Caliciviridae* family [9]. Currently, there are ten genogroups of norovirus, ranging from GI-GX, which are further divided into 48 genotypes [10]. Across the plethora of norovirus genotypes, GI.1 and GII.4, with GI.1 being the laboratory type strain and GII.4 being the most prevalent genotype, are frequently responsible for the majority of infections worldwide [11]. The persistent circulation of various genotypes leads to frequent reinfections, as immunity generated by infection with one genotype provides limited protection against others due to the considerable genetic and antigenic diversity among norovirus strains [4,6]. Therefore, the detection of multiple strains with high sensitivity is vital, given the low infectious dose of the virus [12]. Historically, the lack of a cultivation system for human noroviruses has hindered much of the research surrounding it, including the development of efficient detection systems. Consequently, studies often use related cultivable surrogate viruses, which are organisms used in research to mimic the properties of the virus of interest. Surrogate selection for noroviruses is primarily based on the organism's ability to be propagated in culture, as well as its genetic, physical, or chemical similarity to human noroviruses [13].

Real-time reverse transcription-polymerase chain reaction (RT-PCR) is widely regarded as the "gold standard" for detecting norovirus in both fecal and food samples [14]. Numerous real-time RT-PCR assays are available globally, offering varying levels of sensitivity and selectivity [15]. While advancements can reduce RT-PCR processing time, the need for expensive laboratory equipment, specialized training, and the method's lack of portability limit its applicability in real-world settings [16]. More straightforward immunoassay methods are available, such as commercial enzyme-linked immunosorbent assays (ELISAs) [17–20]. However, these methods often have limitations in sensitivity that reduce their ability to be used for viral detection in foods. Additionally, alternative detection methods are emerging, including electrochemical and colorimetric biosensors [21–23], which vary in sensitivity, capability to detect multiple strains, and portability [23,24]. However, most of these immunoassays and sensors use biological receptors, such as antibodies and peptides, which have several drawbacks. One significant issue is their thermal instability, which requires the assays/reagents to be stored under refrigerated conditions (~4 °C) with a limited shelf-life [25–27]. This temperature sensitivity not only complicates the logistics of storage and transportation but also limits the applicability of these assays in regions with limited resources, contributing to healthcare inequalities.

The inherent complexity of food samples presents additional challenges for developing effective norovirus biosensors and immunoassays. Food matrices often contain a plethora of compounds and have a broad range of pH levels, which can inhibit endpoint detection methods. Although ligand-based methods are often much simpler and faster than DNA-based techniques, developing a universal sensor is challenging [28]. This is because of the highly specific nature of antibodies makes it difficult to achieve broad reactivity across different norovirus strains/-genotypes. This specificity, while advantageous for targeted detection, becomes a limitation when trying to create a sensor capable of recognizing multiple variants, which is particularly where the challenge lies with norovirus detection. Consequently, the use of biological ligand-based assays in food testing can be limited, as careful consideration of these factors is required to ensure reliable and accurate detection.

Due to their synthetic nature, molecularly imprinted polymers (MIPs) possess much greater thermal and chemical stability compared to their biological counterparts [29,30]. These polymers mimic the recognition capabilities of antibodies and comprise of functional monomers, crosslinker monomers, porogens, initiators, and the target analyte. The recognition cavity is formed via the self-assembly of the monomers around the target therefore creating cavities with complementary spatial orientation and functional groups that facilitate a variety of interactions [31,32]. Additionally, a solid-phase approach has been developed to produce molecularly imprinted polymer nanoparticles (nanoMIPs), thus improving template removal, target orientation consistency, and binding site homogeneity [33–35]. NanoMIPs have the key advantage of offering a long shelf life at ambient temperatures and being able to withstand harsh conditions without losing their binding capabilities. Consequently, this makes them ideally suited for integration into portable sensors [29,36].

Combining MIPs with a thermal detection platform has the potential to form an on-site testing system [36–39]. Our previous work demonstrated the ability to easily integrate nanoMIPs into a thermal device via the electrografting of nanoMIPs to low-cost screen-printed graphite electrodes (SPGEs) [38]. The heat transfer method (HTM) measures thermal resistance (R_{th}) at the solid-liquid interface, detecting changes in resistance upon target rebinding. This straightforward method requires minimal training, uses low-cost components, and offers rapid

detection [37]. Previously, we have used nanoMIPs for the electrochemical and thermal detection of norovirus GII.4 [40]. In this work, we have developed novel norovirus nanoMIPs that were produced using a specifically chosen epitope to facilitate cross-reactivity of norovirus GI.1 and GII.4. The selection of the new epitope sequence was derived using literature information on cross-reactive antibodies capable of binding to multiple norovirus genotypes. The nanoMIPs cross reactivity was then investigated against a suite of norovirus strains and common surrogates. This literature highlighted a 10-amino acid sequence as a key binding region from the P1 domain of the GI.1 genotype (SEQAPTVGEA) [41, 42]. Additionally, we explored the practical applicability of this approach for on-site testing by evaluating the detection capability of the nanoMIPs against two prevalent norovirus genotypes and within a relevant food sample. Leafy greens are considered high-risk foods for norovirus contamination due to their frequent raw consumption and large surface area that can easily harbor pathogens, therefore spinach samples were selected [43]. This work showcases the potential of nanoMIPs for in real-world diagnostic settings, addressing both accuracy and ease of deployment in diverse environments. Ultimately, the sensor demonstrated the ability to rapidly detect trace levels of norovirus GI.1 and GII.4 virus-like particles (VLPs) in a food matrix, achieving detection within 30 min alongside achieving limits of detection of 2.19 pg/mL and 2.69 pg/mL for GI.1 and GII.4 VLPs, respectively.

2. Experimental

2.1. Materials

Spheriglass 2429 CP00 glass beads, with a diameter ranging from 53 to 106 μm, were purchased from Blagden Chemicals (Westerham, United Kingdom, UK). 1-ethyl-3-(3-dimethylaminopropyl) carbodiimide (EDC) (CAS:25952-53-8), *N*-hydroxysuccimide (NHS) (98 %, CAS:6066-82-6), PierceTM bicinchoninic acid assay BCA protein assay kit, 4-aminobenzoic acid (4-ABA) (99 %,150-13-0), potassium hexacyanoferrate(II) trihydrate (≥99.5 %, CAS:14459-95-1), potassium ferricyanide(III) (99 %, CAS:13746-66-2), potassium chloride (KCl) (99 %, CAS:7447-40-7), OXOID phosphate buffered saline (PBS) tablets, sodium hydroxide (NaOH) (98 %,1310-73-2), succinimidyl iodoacetate (SIA) (CAS:39028-27-8), acetone (99 %, CAS:67-64-1), isopropanol (extra pure, CAS:67-63-0), sodium nitrite (98 %, CAS:7632-00-0), hydrochloric acid 33 % (HCl), ammonium persulfate (APS) (CAS:7727-54-0), methanol (99.9 %, CAS:67-56-1), acetonitrile (99.9 %, CAS:75-05-8), and anhydrous toluene (99 %, CAS:108-88-3) were acquired from Fisher Scientific (Loughborough, UK). *N*-isopropylacrylamide (NIPAM) (CAS:2210-25-5), *N*-(3-aminopropyl)methacrylamide hydrochloride (NAMPA) (98 %, CAS:72607-53-5), *N,N*′-methylenebisacrylamide (Bis) (99 %, CAS:110-26-9), acrylic acid (AAc) (CAS:79-10-7), *N-tert*-butyl acrylamide (TBAm) (97 %, CAS:107-26-9), *N,N,N*′,*N*′-tetraacetylethylenediamine (TEMED) (99 %, CAS:110-18-9), Supelco polypropylene solid-phase extraction tubes (60 mL), (3-aminopropyl) trimethoxysilane (APTMS) (97 %, CAS:13822-56-5), ethylenediaminetetraacetic acid (EDTA) (99 %, CAS:60-00-4) were obtained from Sigma-Aldrich (Gillingham, UK). All experiments utilized deionized water (DI) with a resistivity of ≥18.2 MΩ cm at 25 °C. The epitope sequence was synthesized and purchased from Abnova (Taipei, Taiwan) via Caltag MedSystems (Buckingham, UK). Recombinant norovirus GI.1 VP1 virus-like particles (VLPs) (100 μg at >90 % purity) were purchased from the native antigen company (Kidlington, UK). Recombinant norovirus GII.4 VP1 virus-like particles (VLPs) with purity >95 % were purchased from Abcam (Cambridge, UK).

Three human norovirus surrogates were used for specificity testing: bacteriophage MS2 (ATCC 15597-B1), Tulane virus (provided courtesy of L.A. Jaykus, N.C. State University), and murine norovirus (ATCC VR-1937). MS2 stocks were prepared using a method adapted from Su et al. [44], in which phages were propagated in *Escherichia coli* C-3000 (ATCC 15597) cultured in tryptic soy broth supplemented with 0.1 % glucose, 2 mM calcium chloride, and 10 μM thiamine. After propagation, cultures were centrifuged to separate cell debris, aliquoted, and stored at −80 °C. Murine norovirus was propagated in RAW 264.7 cells (ATCC TIB-71) grown with Gibco DMEM media supplemented with 10 % FBS, 1 % HEPES, 1 % penicillin-streptomycin, 1 % L-glutamine, and 10 % non-essential amino acids as described in the method reported by Gonzalez-Hernandez et al. [45]. Tulane virus was propagated in LLC-MK2 cells (ATCC CCL-7) grown with Gibco's Medium 199 supplemented with 10 % fetal bovine serum and 1 % penicillin-streptomycin, based on the method first reported by Farkas et al. [46]. Both eukaryotic cell types were cultured in a 37 °C incubator with 5 % CO_2 and were moved to a 32 °C incubator for virus propagation. Upon reaching ~90 % cytopathic effect, cultures were subjected to three freeze-thaw cycles to lyse cells. Cultures were then centrifuged for 5 min at 3000 rpm to pellet cell debris, and virus-containing supernatant was aliquoted and stored long-term at −80 °C.

2.2. NanoMIP synthesis

2.2.1. Rational design

The selected epitope sequence (Fig. 1a) was capped with an additional cysteine to enable attachment to amine-functionalized glass beads using SIA (Fig. 1b) [42]. The predicted epitope structure (Fig. 1a) was modelled using the I-TASSER protein prediction server based on deep-learning models [47]. The linear structure of the epitope minimizes the risk of distortion during the polymerization process, allowing for more accurate cavity formation within the nanoMIP. The functional monomers were selected to achieve a range of potential interactions throughout the amino acid sequence. To promote ionic interactions, AAc and NAMPA were incorporated, while TBAm was included to support hydrophobic interactions. Finally, NIPAM was selected to facilitate hydrogen bonding.

2.2.2. Synthesis of the nanoMIPs

For nanoMIP synthesis, the protocol established by Canfarotta et al. [33] was followed. After the epitope-derivatized beads (60 g) were prepared (see supplementary information for details), the nanoMIPs were then synthesized (Fig. 1c). A monomer solution was prepared containing NIPAM (39 mg), NAMPA (5.3 mg), Bis (2 mg), and AAc (2.2 μL) in 5 mM PBS (99 mL). To this, TBAm (33 mg), dissolved in ethanol (1 mL), was added. The monomer solution was sonicated under vacuum (10 min) and then purged with nitrogen (20 min). Epitope-derivatized glass beads (60 g) were added to the monomer solution with continued nitrogen purging. To initiate the polymerization, a solution of APS (48 mg) and TEMED (30 μL) in DI water (800 μL) was added to the glass beads and monomer solution, continuing nitrogen purging for 10 min. Polymerization was carried out at room temperature (~20 °C) and the solution was incubated for 4 h. Afterward, the glass bead solution was transferred into a 60 mL solid-phase extraction cartridge fitted with a 20 μm porosity frit. The beads were washed with room temperature (~20 °C) DI water (10 × 20 mL) to remove any unreacted monomers and low affinity nanoMIPs. High affinity nanoMIP elution was performed by the addition of 30 mL of prewarmed water (65 °C) and placing the solid-phase extraction cartridge into a water bath set to 65 °C for 30 min. After, this solution was collected under vacuum. The glass beads were further washed with warm water (65 °C) until approximately 150 mL of high affinity nanoMIP solution was collected.

2.3. Characterization

The hydrodynamic diameters of the nanoMIPs were measured using a Malvern Zetasizer Nano ZS (Malvern Panalytical, Malvern, UK). The instrument used a scattering angle of 173° and a laser wavelength of 632.8 nm, performing experiments at 25 ± 0.1 °C. Electrochemical impedance spectroscopy (EIS) measurements were conducted on the Reference 3000™ potentiostat/galvanostat (Gamry Instruments, PA,

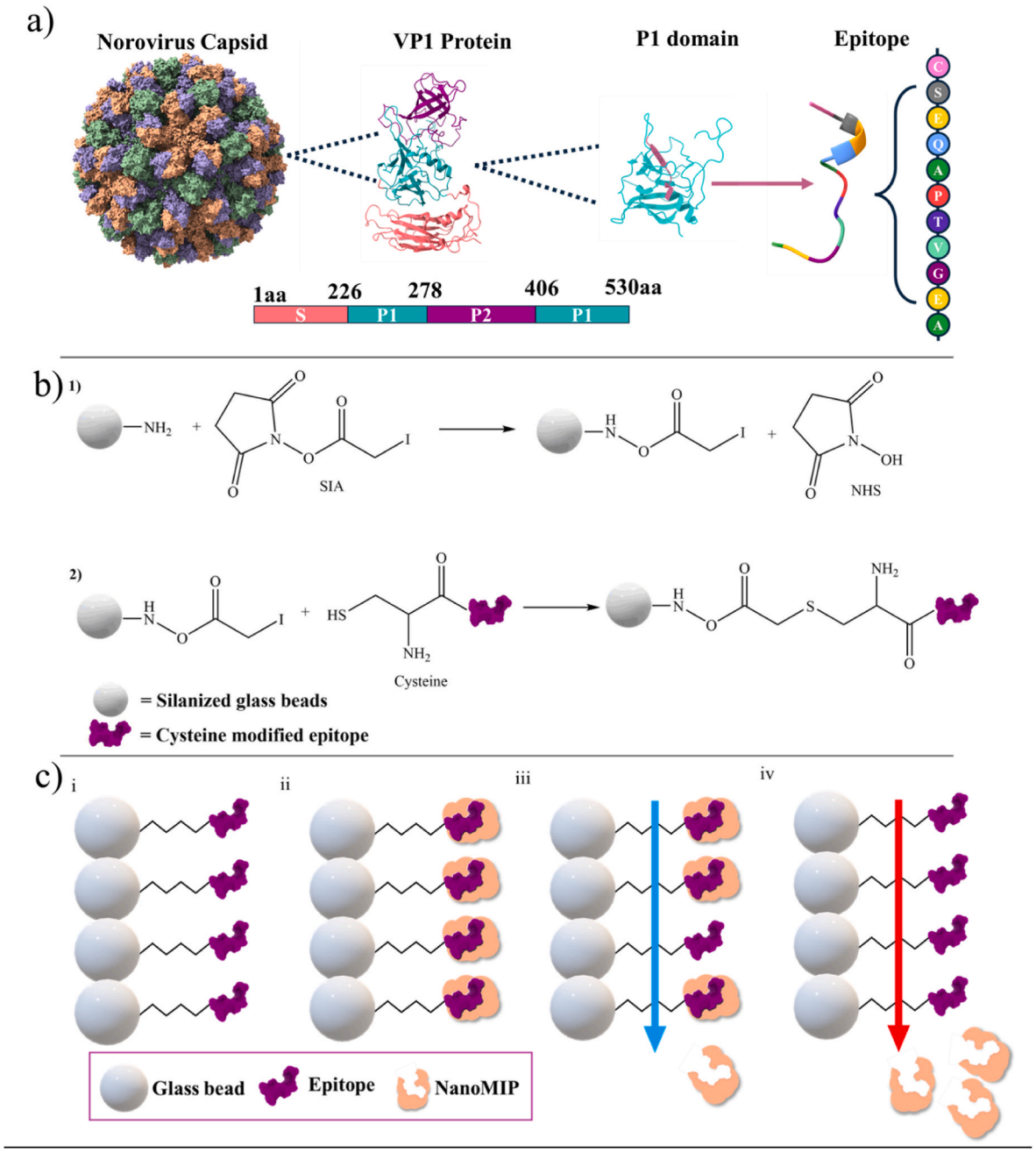

Fig. 1. NanoMIP solid-phase synthesis using epitope imprinting. a) The structure of the norovirus capsid, norovirus VP1 protein, P domain, and epitope sequence/structure (highlighted in pink in previous images). The selected epitope sequence (CSEQAPTVGEA) b) Reaction scheme for coupling the silanized glass beads and the cysteine-capped epitope. c) Solid-phase synthesis: i) Glass beads are activated using NaOH, and then the chosen template is immobilized onto the surface. ii) Polymerization was initiated at room temperature (~20 °C) by sequential addition of functional monomers, crosslinker, and initiator. iii) The beads were washed with water at room temperature (20 °C) to elute any unreacted monomers and low affinity nanoMIPs. iv) High affinity nanoMIPs are eluted using deionized water at 65 °C. (For interpretation of the references to color in this figure legend, the reader is referred to the Web version of this article.)

USA) with an Ag/AgCl reference electrode, an SPGE or glassy carbon electrode as the working electrode, and a Pt wire counter electrode. Measurements were performed at each stage of the immobilization protocol with a fixed frequency range of 0.1 Hz–100 kHz using PBS with $[Fe(CN)_6]^{3-/4-}$ (1 mM) and KCl (0.1 M). Equivalent electrical circuit model fitting was performed using Gamry Echem analyst software. The model included a combination of elements such as solution resistance (R_s), double layer capacitance (C_{dl}), and Warburg resistance (W), which was used to calculate charge transfer resistance (R_{ct}).

2.4. Electrografting

To adhere the nanoMIPs to the surface of the electrode (SPGEs/glassy carbon electrode), an electrografting method developed in previous work was used [38]. The SPGEs were produced by screen-printing a graphite ink formulation (Gwent Electronic Materials Ltd., Monmouthshire, UK) onto a polyester substrate, followed by curing at 60 °C for 30 min. The SPGEs were submerged in a solution of 4-ABA (2 mM) and sodium nitrite (2 mM) in aqueous HCl (0.5 M) while cyclic voltammetry was performed from +0.2 V to −0.6 V at 100 mV/s. The SPGE was removed from the solution, rinsed with DI water, and dried with

nitrogen. A solution of EDC (100 mM) and NHS (20 mM) in PBS, adjusted with HCl to pH 5, was prepared and drop cast (8 μL) onto the working surface of the SPGE and left for 1 h. Afterward, the SPGE was washed with DI water and gently dried with nitrogen before 8 μL of the nanoMIP solution was added to the surface. This was left to incubate for 3 h at room temperature and then rinsed with the DI water to remove any excess material.

2.5. Epitope rebinding

To achieve initial conformation of binding between the nanoMIPs and epitope, EIS was employed with a functionalized glassy carbon electrode. Using the same parameters as stated in Section 2.4, the R_{ct} of the nanoMIP-functionalized electrode was measured. Epitope solutions in PBS, with concentrations ranging from 1 to 10,000 pg/mL, were prepared and incrementally added (10 μL) to the electrode surface, allowing a 10 min incubation period. Prior to each measurement, the electrode was rinsed with DI water to remove any unbound material. Calibration plots were then generated based on the change in R_{ct} upon the rebinding of the epitope relative to the baseline of the functionalized electrode.

2.6. Thermal detection

A resin measurement cell was fabricated using an Anycubic Photon 3D Mono 4K printer with Anycubic clear standard resin (Shenzhen, China). The cells were designed in Blender 3.0.0 with external dimensions of 18.2 mm (W) × 30.0 mm (L) × 10.3 mm (D), featuring an internal liquid reservoir with a diameter of 5.7 mm (Fig. 2) [48]. Slicing was performed using Lychee Slicer 7.1, where bottom layer exposure was set to 25 s and normal layer exposure was set to 2.8 s. Immediately after printing, the cells were washed in isopropanol for 20 min and cured for 6 min using an Anycubic Wash & Cure device. A nanoMIP-functionalized SPGE was placed on the copper block, with an O–ring positioned above to form a sealed sample reservoir (Fig. 2a). The cell was then secured tightly with four nuts and bolts. The device was controlled using LabView software and a proportional-integral-derivative (PID) controller attached to a power resistor (22 Ω). Two Type K thermocouples (RS Components, London, UK) were used: T_1 was inserted into the copper block, which acted as a heat sink, and T_2 was placed into the sample chamber (Fig. 2b). The PID controller regulated the temperature of the copper block (T_1), which was maintained at 37.0 ± 0.02 °C [39]. The thermal resistance (R_{th}, °C/W) at the solid-liquid interface was determined by subtracting the temperature of the sample (T_2) from the temperature of the copper block (T_1) and dividing this difference by the power input (P) required to keep T_1 constant.

$$R_{th} = \frac{(T_1 - T_2)}{P} \qquad \text{Equation 1}$$

For the measurements, PBS solution (150 μL) was initially pipetted into the reservoir, and the thermal resistance signal was allowed to stabilize for 15 min. The reference solution was then removed using a pipette, and the sample (150 μL) was added. The change in thermal resistance (ΔR_{th}) was calculated by subtracting the sample R_{th} for the PBS baseline signal. The normalized thermal resistance was considered to eliminate the influence of external factors. Measurements of epitope samples were taken in triplicate using the concentrations stated in section 2.5. Spiked samples of VLPs were produced (0.1–1000 pg/mL or 5.7 × 10^3 - 5.7 × 10^7 particles/mL) with measurements performed in triplicate. The limit of detection (LoD) was calculated by utilizing the three-sigma technique ($3\sigma/S$), where σ is the standard deviation of the baseline of a blank concentration of analyte, and S is the slope of the calibration plot.

Spinach was selected for this study to replicate real-life contamination scenarios. A solution of 10:1 (w/w) of PBS and chopped spinach, purchased from a local store (Marks & Spencer, Newcastle, UK), was prepared. Following our previously established protocol [40], the vial contents were thoroughly mixed using an orbital shaker at 75 rpm for 5 min, followed by vortex mixing for 30 s and sonication for 480 s. The mixing procedure was performed twice, after which the sample was filtered through a 10 μm mesh before use. With this solution, spiked samples of VLPs were produced at the same concentrations as previous experiments (0.1–1000 pg/mL), and measurements were performed in triplicate. For each surrogate experiment, Tulane virus, murine norovirus, and bacteriophage MS2 dilutions in spiked PBS were produced with measurements performed in triplicate. Paired t-tests were performed, assuming normal distribution and equivalent standard deviation. Using a basic local alignment search tool (BLAST), the sequence similarity of the capsid proteins was determined.

3. Results and discussion

3.1. NanoMIP and functionalized electrode characterisation

The nanoMIPs were synthesized using the epitope sequence immobilized on a solid-phase support and subsequently eluted through a two-step process. Using dynamic light scattering, we measured the hydrodynamic diameter (D_h) of the nanoMIPs to be 178 nm (Fig. 3a). The nanoMIPs also exhibited a polydispersity index of 0.217, indicating a narrow size distribution and, thus, a high degree of homogeneity. This uniformity in nanoMIP size is essential in achieving consistent and reproducible sensing performance. Free carboxylic acid groups were introduced to the SPGE surface via the electrografting of 4-aminobenzoic acid (4-ABA). The nanoMIPs were then attached via EDC/NHS coupling utilizing a free amine group (Fig. 3b). The decreasing current observed with each successive scan indicates the progressive deposition of 4-ABA, demonstrating the modification to the electrode surface (Fig. 3c). To confirm the attachment of nanoMIPs to the SPGEs, EIS was used to obtain Nyquist plots for each stage of the electrografting process

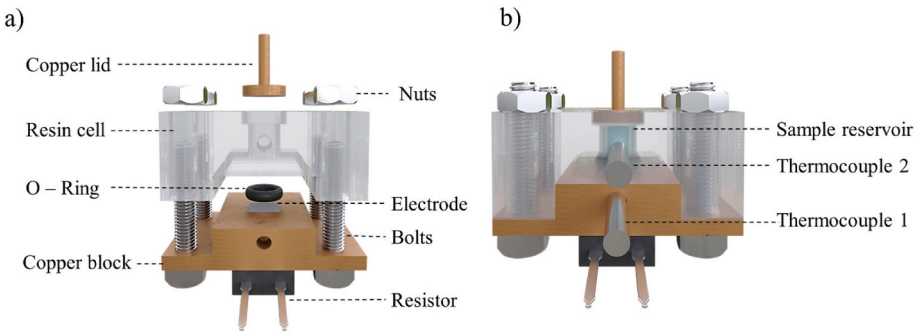

Fig. 2. Schematic design of the thermal measurement cell. a) Configuration of the 3D-printed cell, a copper lid, the functionalized SPGE, and a copper heat sink to which a resistor is attached. b) The cell is sealed for measurements, and two thermocouples are added.

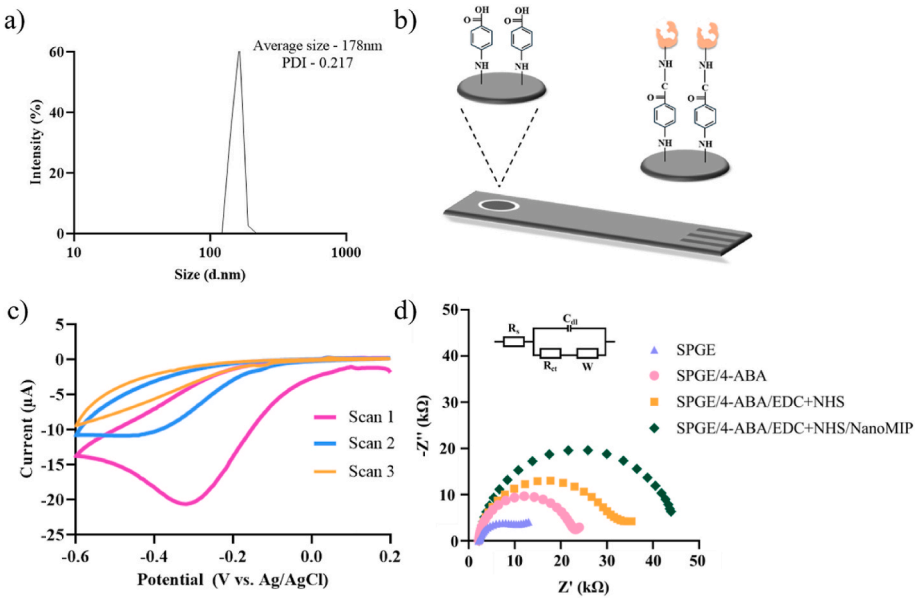

Fig. 3. a) Dynamic light scattering spectrum. of the nanoMIPs in DI water. b) Schematic diagram showing nanoMIP coupling to SPGEs. c) Cyclic voltammogram showing the electrodeposition of 4-ABA onto the SPGEs. d) Nyquist plots from EIS confirming the successful immobilization of nanoMIPs to SPGEs. The plots show a progressive increase in R_{ct} at each stage of the process: 1) blank SGPE (blue triangles), 2) electrografting of 4-ABA onto the SPGE (pink circles), 3) addition of EDC/NHS (orange squares), and 4) nanoMIP coupling (green diamonds). (For interpretation of the references to color in this figure legend, the reader is referred to the Web version of this article.)

to monitor changes in R_{ct} throughout the process (Fig. 3d). At each stage, the increase in resistance arises from the formation of an additional layer, which hinders electron transfer (Table S1).

3.2. Epitope rebinding

EIS was employed as a screening technique, using a glassy carbon electrode, to confirm the rebinding capabilities of the nanoMIPs to their targeted epitope and the formation of complementary binding sites within the nanoMIPs. The R_{ct} values increased with increasing epitope concentration (Fig. S1a and b), which can be attributed to the epitope binding to the nanoMIP-functionalized electrode, obstructing electron flow from the redox solution ($[Fe(CN)_6]^{3-/4-}$). A corresponding dose-response curve demonstrated (Fig. S1b) that the nanoMIPs could successfully rebind the target epitope across a wide concentration range (1–100000 pg/mL). These results, obtained using a well-established electrochemical technique, confirmed the effective binding capability of the nanoMIPs. This validation provided the basis for their integration into the bespoke thermal sensor, where epitope rebinding studies were subsequently repeated. The thermal experiments shifted to the use of SPGEs based on their low-cost and ease of integration into the thermal device. The increasing epitope concentrations resulted in a stepwise increase in R_{th} with an LoD of 0.79 pg/mL (Fig. S1c and d). After confirming successful rebinding through EIS and thermal detection, the system was validated for subsequent virus-like particle (VLP) thermal analysis.

3.3. Virus particle detection

After confirmation of the detection of the target epitope, experiments were repeated using VLPs, which consist of the fully assembled viral capsid without the internal genetic material, to better reflect real-world measurements. Therefore, thermal experiments were performed using a wide concentration range of VLP-spiked PBS solutions (0.1–1000 pg/mL). A monotonic increase in R_{th} with increasing VLP concentration was observed, which can be attributed to VLPs binding to nanoMIPs on the SPGE surface. Both GI.1 and GII.4 strains exhibited similar binding responses, with consistent changes in R_{th} observed across the analysis range (Fig. 4). The sensor exhibited LoD of 1.53 pg/mL (0.87×10^5 particles/mL) for GI.1 and 2.28 pg/mL (1.30×10^5 particles/mL) for GII.4. The LoD achieved in this work improves upon our prior study, where thermal detection of GII.4 yielded a LoD of 6.5 pg/mL. The results highlight the sensor's ability to detect two genotypes of norovirus using a single ligand, representing an important advancement on our previous work. The ability to detect noroviruses from two genogroups greatly enhances the practicality of the sensor as it allows for broader detection of noroviruses, without requiring multiple assays. The similarity in amino acid sequences within the selected P1 domain of the two strains (Table S4) is likely to enable the binding. While sensors capable of detecting multiple strains have been developed, they can face challenges, such as requiring specialized training and utilizing biological receptors, which limits their practicality [49,50]. The total time needed to complete the analysis using our sensor (30 min) is significantly shorter than that of RT-PCR methods (several hours) [51]. Furthermore, our sensor exhibits a lower LoD compared to traditional ELISA assays [51–54] and a comparable LoD to alternative emerging biosensors in the literature, such as lateral flow and colorimetric assays (Table S5) [54,55].

3.4. Surrogate selectivity

The selectivity of the nanoMIPs was explored by repeating thermal measurements using a panel of viruses that progressively differ genetically from the GI.1 strain used to imprint the nanoMIPs (Table S2). Based on the molecular weight of the VP1 protein (~59 kDa) and that each VLP consists of 180 copies of VP1, the total weight of one VLP is estimated at 10.62 MDa. The VLP concentration could then be converted to particles/mL, enabling comparisons with other molecules. The thermal responses (Fig. 5a) for murine norovirus, Tulane virus, and bacteriophage MS2 showed a statistically significant difference (Table S3) when compared to the GI.1 VLPs, reflecting the increased genetic divergence of these viruses (Fig. 5b). Murine Norovirus, while still belonging to the Norovirus genus, showed a reduction in ΔR_{th} compared to GI.1 and GII.4. The genetic variations among viruses can be quantitatively assessed by analyzing differences in the amino acid sequences of their capsid proteins. Norovirus GII.4 and murine norovirus showed 44

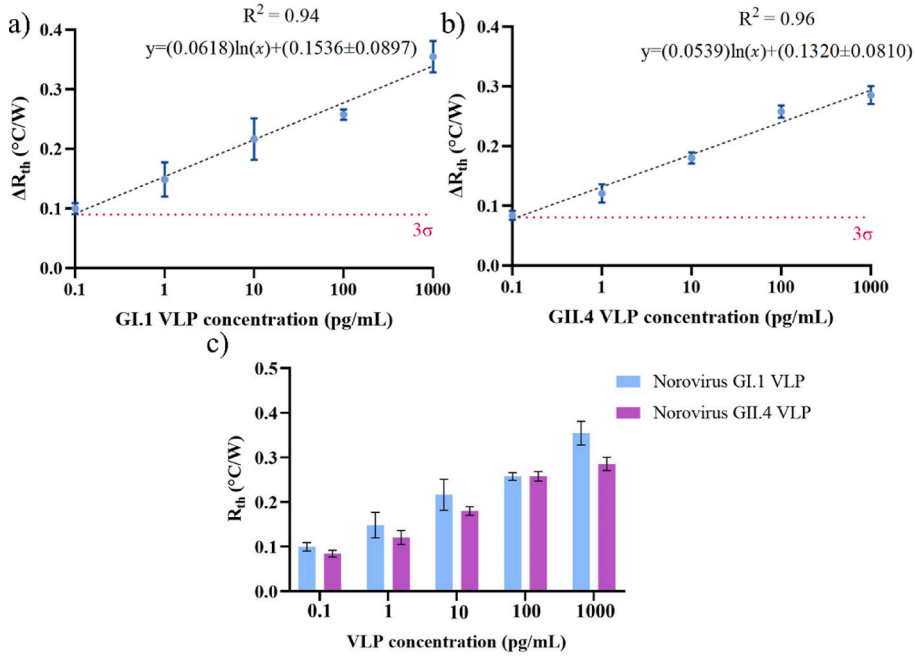

Fig. 4. a and b) Dose–response curves of SPGEs functionalized with nanoMIPs upon addition of VLP concentrations and the ΔR_{th} for two norovirus genotypes, GI.1 and GII.4, in a PBS solution. The error bars represent the standard deviation of the three repeats with the pink dotted line representing three times the baseline standard deviation of the control injection c) A comparative bar chart of the results for the two strains. (For interpretation of the references to color in this figure legend, the reader is referred to the Web version of this article.)

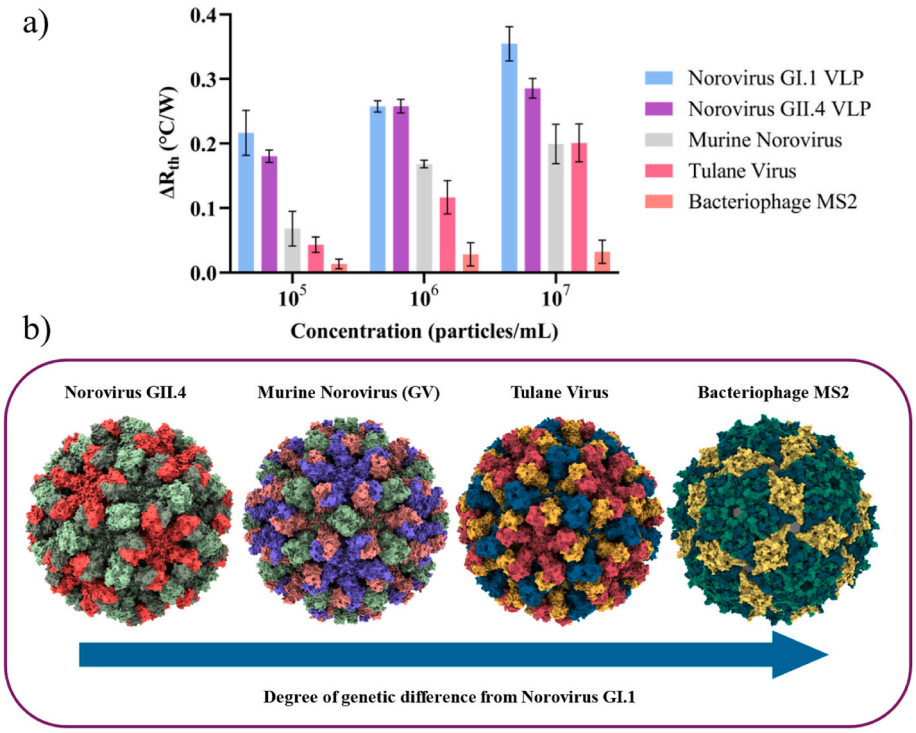

Fig. 5. a) Mean ΔR_{th} for Norovirus GI.1 VLP, Norovirus GII.4 VLP, Murine Norovirus, Tulane Virus, and Bacteriophage MS2 with error bars representing the standard deviation of the three repeats. b) Models of the capsids of each virus in order of genetic difference from Norovirus GI.1 reproduced using data from RCSB Protein Data Bank (RCSB PDB) [56–59].

% and 40 % amino acid similarity to GI.1, respectively. The selected epitope region exhibits similarities between GI.1 and GII.4 (Table S4), whereas the reduced response of murine norovirus may be due to much of the sequence similarity being located in the shell domain or non-binding regions, leaving key differences in the binding region critical for interaction with the sensor. Tulane virus capsid protein was calculated to have a 29 % similarity which reflects the reduced response of the sensor. Bacteriophage MS2, the most genetically distant virus in the

panel, displayed no significant similarity and produced the smallest change in thermal resistance, indicating selectivity of the nanoMIPs for members of the *Caliciviridae* family and reduced response to other viruses that have similar capsid symmetry and structural properties. Interestingly, the fact that some cross-reactivity was observed with murine norovirus and Tulane virus suggests that nanoMIPs may be well suited as ligands for broad detection of diverse pathogens in general.

3.5. Food samples

To further evaluate the sensor's suitability, nanoMIP performance was evaluated in a representative food sample, specifically spinach rinsate. The spinach rinsate preparation simply required combining the spinach with PBS and agitating. The change in color and pH of the solution (Fig. 6a), along with the increase in R_{th} of spinach samples (Fig. 6b), indicates the addition of food matrix components, such as proteins and carbohydrates into the suspension. Across the three ratios of PBS to spinach, 50:1, 25:1, and 10:1, the baseline standard deviations over a 100-s period were 0.0295, 0.0296, and 0.0308, respectively (Fig. S2). A 10:1 ratio of PBS to spinach was selected as, even with the highest percentage of food content, this ratio maintained the stable baseline necessary for the experiments. To further evaluate the sensor's suitability, the spinach rinsate samples were spiked with VLPs (0.1–1000 pg/mL) and analyzed as a representative practical sample. The cumulative addition of increasingly concentrated VLP solutions demonstrated a stepwise increase in R_{th} (Fig. 6c). Dose-response curves showed linear detection across a concentration range spanning many orders of magnitude (Fig. 6e and f). The obtained LoD values in the spinach rinsate were 2.19 pg/mL (1.25×10^5 particles/mL) for norovirus GI.1 and 2.69 pg/mL (1.53×10^5 particles/mL) for norovirus GII.4. These thermal detection results and corresponding LoD values were very similar to those obtained when using only spiked-PBS, which demonstrates the nanoMIPs retain their excellent sensing performance even within a complex food matrix. This work provides further support for the excellent stability and robustness of the nanoMIPs in food samples, creating high potential for expanding the sensor into other food matrices. Moreover, achieving detection within 30 min (Fig. 6d) is significantly faster than alternative methods, demonstrating the nanoMIP sensors' potential for rapid detection and making it highly suitable for on-site testing applications.

4. Conclusions

In this work, we have advanced the development of an on-site norovirus sensor based upon polymeric recognition elements integrated into a thermal detection method. By using epitope imprinting, nanoMIPs were successfully imprinted with a short amino acid sequence derived from the more conserved region of the norovirus capsid protein. As a result, the nanoMIPs successfully demonstrated rebinding of the epitope and subsequent binding to norovirus GI.1 and GII.4 VLPs. This method

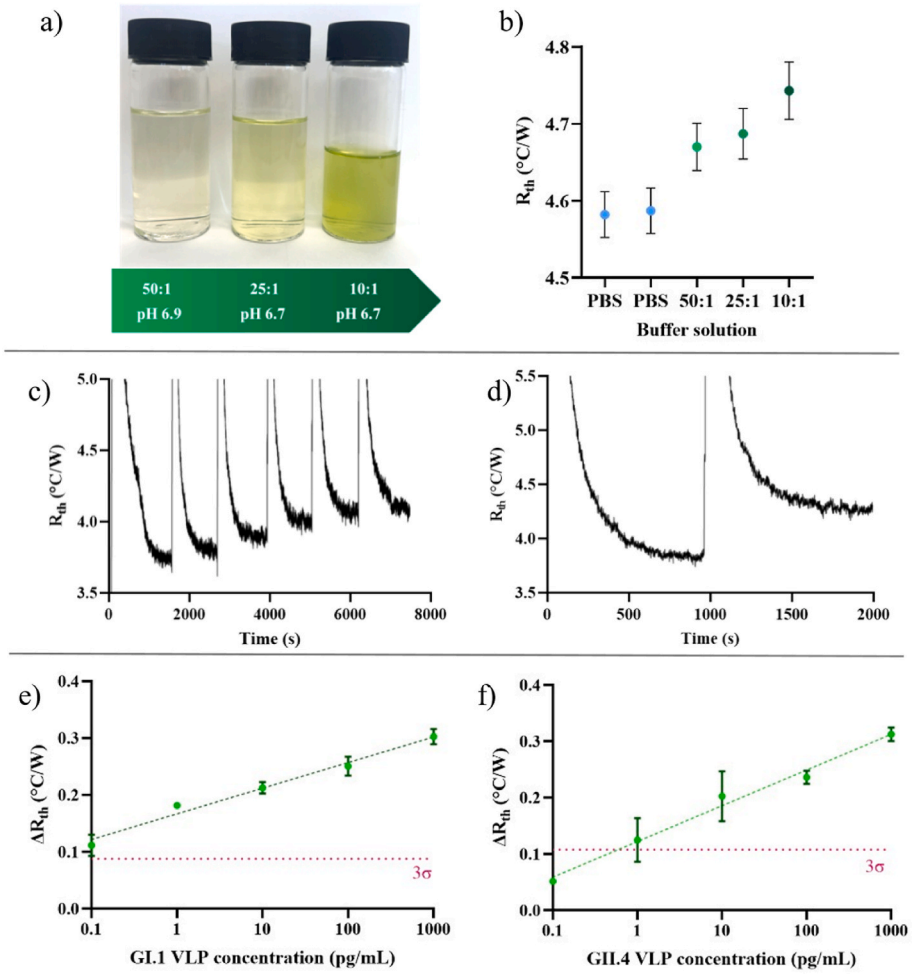

Fig. 6. a) Three ratios of PBS:spinach solutions. b) Baseline R_{th} of standard PBS and PBS:spinach ratios. c) Example of raw thermal data of increasing concentrations of VLPs in PBS:spinach d) Example of detection in spinach showing the baseline and VLP detection. e and f) Dose–response curve of GI.1 and GII.4 VLP concentrations. The error bars represent the standard deviation of the three repeats with the pink dotted line representing the baseline standard deviation of the control injection multiplied by three. (For interpretation of the references to color in this figure legend, the reader is referred to the Web version of this article.)

achieved favorable LoDs, of 1.53 and 2.28 pg/mL for GI.1 and GII.4 VLPs in the control buffer, respectively. Comparable LoDs were observed in spinach samples, with values of 2.19 and 2.69 pg/mL, demonstrating consistency across matrices. This supports the method's applicability for real-world norovirus detection in contaminated food samples. By flagging samples that may harbor these common norovirus strains, our sensor has the potential to enable timely interventions to prevent outbreaks. Importantly, this method provides a rapid analysis protocol with detection completed within 30 min along with simple sample preparation. This work further demonstrates that a small target epitope can be used to generate norovirus ligands with cross-genogroup binding activity. This has implications for future work in the development of ligands, as such a short peptide epitope can be readily synthesized compared to other traditional targets. Further, the ability to generate ligands that have affinity for GI and GII genogroups has been a challenge in detection; however, the work reported here suggests that nanoMIPs may display an ideal balance of allowing broad reactivity of noroviruses at the genogroup level while still maintaining specificity to non-target proteins that are closely related. Further, the ability to withstand a complex matrix suggests that this technology also could show particular promise for in-field detection of viruses in foods with crude sample processing in a truly portable manner.

CRediT authorship contribution statement

Amy Dann: Writing – review & editing, Writing – original draft, Methodology, Investigation, Formal analysis, Data curation. **Pankaj Singla:** Writing – review & editing, Supervision, Methodology, Investigation, Formal analysis, Data curation. **Jake McClements:** Writing – review & editing, Writing – original draft, Supervision, Resources, Funding acquisition, Formal analysis, Conceptualization. **Minji Kim:** Writing – review & editing, Resources, Investigation, Formal analysis. **Sloane Stoufer:** Writing – review & editing, Resources, Methodology, Investigation, Data curation. **Robert D. Crapnell:** Writing – review & editing, Supervision, Resources, Investigation, Formal analysis, Data curation. **Craig E. Banks:** Writing – review & editing, Supervision, Resources, Project administration, Funding acquisition. **Shayan Seyedin:** Writing – review & editing, Supervision, Project administration, Methodology, Investigation, Formal analysis. **Mark Geoghegan:** Writing – review & editing, Supervision, Methodology. **Christopher F. Blanford:** Writing – review & editing, Supervision, Project administration, Methodology, Investigation, Formal analysis. **Matthew D. Moore:** Writing – review & editing, Writing – original draft, Supervision, Resources, Project administration, Methodology, Investigation, Funding acquisition, Formal analysis, Conceptualization. **Marloes Peeters:** Writing – review & editing, Writing – original draft, Supervision, Resources, Project administration, Methodology, Investigation, Funding acquisition, Formal analysis, Conceptualization.

Declaration of competing interest

The authors declare that they have no known competing financial interests or personal relationships that could have appeared to influence the work reported in this paper.

Acknowledgements

This work was supported by the USDA National Institute of Food and Agriculture, AFRI project 2022-67021-36408.

Appendix A. Supplementary data

Supplementary data to this article can be found online at https://doi.org/10.1016/j.aca.2025.344331.

Data availability

Data will be made available on request.

References

[1] A.S. Daar, H. Thorsteinsdóttir, D.K. Martin, A.C. Smith, S. Nast, P.A. Singer, Top ten biotechnologies for improving health in developing countries, Nat. Genet. 32 (2002) 229–232, https://doi.org/10.1038/ng1002-229.
[2] M.Y.-C. Wu, M.-Y. Hsu, S.-J. Chen, D.-K. Hwang, T.-H. Yen, C.-M. Cheng, Point-of-Care detection devices for food safety monitoring: proactive disease prevention, Trends Biotechnol. 35 (2017) 288–300, https://doi.org/10.1016/j.tibtech.2016.12.005.
[3] P. LeDuc, M. Agaba, C.-M. Cheng, J. Gracio, A. Guzman, A. Middelberg, Beyond disease, how biomedical engineering can improve global health, Sci. Transl. Med. 6 (2014), https://doi.org/10.1126/scitranslmed.3009067.
[4] M.D. Moore, R.M. Goulter, L.-A. Jaykus, Human norovirus as a foodborne pathogen: challenges and developments, Annu. Rev. Food Sci. Technol. 6 (2015) 411–433, https://doi.org/10.1146/annurev-food-022814-015643.
[5] E. Scallan, R.M. Hoekstra, F.J. Angulo, R.V. Tauxe, M.-A. Widdowson, S.L. Roy, et al., Foodborne illness acquired in the united states—major pathogens, Emerg. Infect. Dis. 17 (2011) 7–15, https://doi.org/10.3201/eid1701.P11101.
[6] B. Lopman, Global Burden of Norovirus and Prospects for Vaccine Development, CDC, 2015.
[7] S. Rouhani, P. Peñataro Yori, M. Paredes Olortegui, M. Siguas Salas, D. Rengifo Trigoso, D. Mondal, et al., Norovirus infection and acquired immunity in 8 countries: results from the MAL-ED study, Clin. Infect. Dis. 62 (2016) 1210–1217, https://doi.org/10.1093/cid/ciw072.
[8] NIHR, UK's first norovirus mRNA vaccine trial launched. https://www.nihr.ac.uk/news/uks-first-norovirus-mrna-vaccine-trial-launched, 2024. (Accessed 1 November 2024).
[9] Y. Lucero, D.O. Matson, S. Ashkenazi, S. George, M. O'Ryan, Norovirus, Facts and reflections from past, present, and future, Viruses 13 (2021) 2399, https://doi.org/10.3390/v13122399.
[10] P. Chhabra, M. de Graaf, G.I. Parra, M.C.-W. Chan, K. Green, V. Martella, et al., Updated classification of norovirus genogroups and genotypes, J. Gen. Virol. 100 (2019) 1393–1406, https://doi.org/10.1099/jgv.0.001318.
[11] N. Winder, S. Gohar, M. Muthana, Norovirus: an overview of virology and preventative measures, Viruses 14 (2022) 2811, https://doi.org/10.3390/v14122811.
[12] E. Robilotti, S. Deresinski, B.A. Pinsky, Norovirus, Clin. Microbiol. Rev. 28 (2015) 134–164, https://doi.org/10.1128/CMR.00075-14.
[13] G.P. Richards, Critical review of norovirus surrogates in food safety research: rationale for considering volunteer studies, Food Environ. Virol. 4 (2012) 6–13, https://doi.org/10.1007/s12560-011-9072-7.
[14] K. Kumthip, P. Khamrin, W. Saikruang, K. Supadej, H. Ushijima, N. Maneekarn, Comparative evaluation of norovirus infection in children with acute gastroenteritis by rapid immunochromatographic test, RT-PCR and real-time RT-PCR, PLoS One 8 (2021), https://doi.org/10.1371/journal.pone.0248581.
[15] K. Rupprom, P. Chavalitshewinkoon-Petmitr, P. Diraphat, L. Kittigul, Evaluation of real-time RT-PCR assays for detection and quantification of norovirus genogroups I and II, Virol. Sin. 32 (2017) 8.
[16] N. Jothikumar, J.A. Lowther, K. Henshilwood, D.N. Lees, V.R. Hill, J. Vinjé, Rapid and sensitive detection of noroviruses by using TaqMan-Based one-step reverse Transcription-PCR assays and application to naturally contaminated shellfish samples, Appl. Environ. Microbiol. 71 (2005) 1870–1875, https://doi.org/10.1128/AEM.71.4.1870-1875.2005.
[17] S.G. Morillo, A. Luchs, A. Cilli, C.D. Ribeiro, S.J. Calux, R. de CC. Carmona, et al., Norovirus 3rd generation kit: an improvement for rapid diagnosis of sporadic gastroenteritis cases and valuable for outbreak detection, J. Virol. Methods 173 (2011) 13–16, https://doi.org/10.1016/j.jviromet.2010.12.017.
[18] A. Dimitriadis, J.A. Marshall, Evaluation of a commercial enzyme immunoassay for detection of norovirus in outbreak specimens, Eur. J. Clin. Microbiol. Infect. Dis. 24 (2005) 615–618, https://doi.org/10.1007/s10096-005-0012-z.
[19] K. Ambert-Balay, P. Pothier, Evaluation of 4 immunochromatographic tests for rapid detection of norovirus in faecal samples, J. Clin. Virol. 56 (2013) 278–282, https://doi.org/10.1016/j.jcv.2012.11.001.
[20] J.J. Gray, E. Kohli, F.M. Ruggeri, H. Vennema, A. Sanchez-Fauquier, E. Schreier, et al., European multicenter evaluation of commercial enzyme immunoassays for detecting norovirus antigen in fecal samples↻, Clin. Vaccine Immunol. 14 (2007) 7.
[21] M. Zaczek-Moczydlowska, M.A. Zaczek-Moczydłowska, A. Beizaei, M. Dillon, Michael Dillion, K. Campbell, et al., Current state-of-the-art diagnostics for norovirus detection: model approaches for point-of-care analysis, Trends Food Sci. Technol. 114 (2021) 684–695, https://doi.org/10.1016/j.tifs.2021.06.027.
[22] P. Weerathunge, R. Ramanathan, V.A. Torok, K. Hodgson, Y. Xu, R. Goodacre, et al., Ultrasensitive colorimetric detection of murine norovirus using NanoZyme aptasensor, Anal. Chem. 91 (2019) 3270–3276, https://doi.org/10.1021/acs.analchem.8b03300.
[23] H.J. Hwang, M.Y. Ryu, C.Y. Park, J. Ahn, H.G. Park, C. Choi, et al., High sensitive and selective electrochemical biosensor: label-Free detection of human norovirus using affinity peptide as molecular binder, Biosens. Bioelectron. 87 (2017) 164–170, https://doi.org/10.1016/j.bios.2016.08.031.

[24] N. Wang, G. Pan, S. Guan, S. Rong, D. Wang, Z. Gao, et al., A broad-range disposable electrochemical biosensor based on screen-printed carbon electrodes for detection of human noroviruses, Front. Bioeng. Biotechnol. 10 (2022) 845660, https://doi.org/10.3389/fbioe.2022.845660.
[25] F. He, S. Hogan, R.F. Latypov, L.O. Narhi, V.I. Razinkov, High throughput thermostability screening of monoclonal antibody formulations, J. Pharmaceut. Sci. 99 (2010) 1707–1720, https://doi.org/10.1002/jps.21955.
[26] I. Chianella, A. Guerreiro, E. Moczko, J.S. Caygill, E.V. Piletska, I.M.P. De Vargas Sansalvador, et al., Direct replacement of antibodies with molecularly imprinted polymer nanoparticles in ELISA—Development of a novel assay for vancomycin, Anal. Chem. 85 (2013) 8462–8468, https://doi.org/10.1021/ac402102j.
[27] Wantai SARS-CoV-2 Diagnostics, WANTAI SARS-CoV-2 Ab rapid test. https://www.fda.gov/media/140030/download, 2021. (Accessed 22 January 2023).
[28] L. Liu, Lingling Liu, M.D. Moore, A survey of analytical techniques for noroviruses, Foods 9 (2020) 318, https://doi.org/10.3390/foods9030318.
[29] J. Svenson, I.A. Nicholls, On the thermal and chemical stability of molecularly imprinted polymers, Anal. Chim. Acta 435 (2001) 19–24, https://doi.org/10.1016/S0003-2670(00)01396-9.
[30] A. Dann, S. Kaur, S. Stoufer, M. Kim, I. Kaur, M.D. Moore, et al., Molecularly imprinted polymers for detection of chemical and microbial contaminants in foods. Ref. Module Food Sci., Elsevier, 2023, https://doi.org/10.1016/B978-0-12-822521-9.00186-6. B9780128225219001866.
[31] M. Maeda, R.A. Bartsch, Molecular and ionic recognition with imprinted polymers, ACS Symp Ser Am Chem Soc 8 (1998).
[32] J.J. BelBruno, Molecularly imprinted polymers, Chem Rev 26 (2019).
[33] F. Canfarotta, A. Poma, A. Guerreiro, S. Piletsky, Solid-phase synthesis of molecularly imprinted nanoparticles, Nat. Protoc. 11 (2016) 443–455, https://doi.org/10.1038/nprot.2016.030.
[34] J. Wackerlig, P.A. Lieberzeit, Molecularly imprinted polymer nanoparticles in chemical sensing – Synthesis, characterisation and application, Sens Actuators B Chem 207 (2015) 144–157, https://doi.org/10.1016/j.snb.2014.09.094.
[35] S. Ambrosini, S. Beyazit, K. Haupt, B. Tse Sum Bui, Solid-phase synthesis of molecularly imprinted nanoparticles for protein recognition, Chem Commun 49 (2013) 6746, https://doi.org/10.1039/c3cc41701h.
[36] J. McClements, L. Bar, P. Singla, F. Canfarotta, A. Thomson, J. Czulak, et al., Molecularly imprinted polymer nanoparticles enable rapid, reliable, and robust point-of-care thermal detection of SARS-CoV-2, ACS Sens. 7 (2022) 1122–1131, https://doi.org/10.1021/acssensors.2c00100.
[37] O. Jamieson, K. Betlem, N. Mansouri, R.D. Crapnell, F.S. Vieira, A. Hudson, et al., Electropolymerised molecularly imprinted polymers for the heat-transfer based detection of microorganisms: a proof-of-concept study using yeast, Therm. Sci. Eng. Prog. 24 (2021) 100956, https://doi.org/10.1016/j.tsep.2021.100956.
[38] J. McClements, P.M. Seumo Tchekwagep, A.L. Vilela Strapazon, F. Canfarotta, A. Thomson, J. Czulak, et al., Immobilization of molecularly imprinted polymer nanoparticles onto surfaces using different strategies: evaluating the influence of the functionalized interface on the performance of a thermal assay for the detection of the cardiac biomarker troponin I, ACS Appl. Mater. Interfaces 13 (2021) 27868–27879, https://doi.org/10.1021/acsami.1c05566.
[39] R.D. Crapnell, F. Canfarotta, J. Czulak, R. Johnson, K. Betlem, F. Mecozzi, et al., Thermal detection of cardiac biomarkers heart-fatty acid binding protein and ST2 using a molecularly imprinted nanoparticle-based multiplex sensor platform, ACS Sens. 4 (2019) 2838–2845, https://doi.org/10.1021/acssensors.9b01666.
[40] S. Kaur, P. Singla, A.J. Dann, J. McClements, M.V. Sullivan, M. Kim, et al., Sensitive electrochemical and thermal detection of human noroviruses using molecularly imprinted polymer nanoparticles generated against a viral target, ACS Appl. Mater. Interfaces (2024), https://doi.org/10.1021/acsami.4c01942 acsami.4c01942.
[41] B. Kou, S.E. Crawford, N.J. Ajami, R. Czakó, F.H. Neill, T.N. Tanaka, et al., Characterization of cross-reactive norovirus-specific monoclonal antibodies, Clin. Vaccine Immunol. 22 (2015) 160–167, https://doi.org/10.1128/CVI.00519-14.
[42] S.E. Crawford, N. Ajami, T.D. Parker, N. Kitamoto, K. Natori, N. Takeda, et al., Mapping broadly reactive norovirus genogroup I and II monoclonal antibodies, Clin. Vaccine Immunol. 22 (2015) 168–177, https://doi.org/10.1128/CVI.00520-14.
[43] E. DiCaprio, A. Purgianto, Y. Ma, J. Hughes, X. Dai, J. Li, Attachment and localization of human norovirus and animal caliciviruses in fresh produce, Int. J. Food Microbiol. 211 (2015) 101–108, https://doi.org/10.1016/j.ijfoodmicro.2015.07.013.
[44] X. Su, S. Zivanovic, D.H. D'Souza, Effect of chitosan on the infectivity of murine norovirus, Feline calicivirus, and bacteriophage MS2, J Food Prot 72 (2009) 2623–2628, https://doi.org/10.4315/0362-028x-72.12.2623.
[45] M.B. Gonzalez-Hernandez, J. Bragazzi Cunha, C.E. Wobus, Plaque assay for murine norovirus, J Vis Exp JoVE e4297 (2012), https://doi.org/10.3791/4297.
[46] T. Farkas, K. Sestak, C. Wei, X. Jiang, Characterization of a rhesus monkey calicivirus representing a new genus of caliciviridae, J. Virol. 82 (2008) 5408–5416, https://doi.org/10.1128/jvi.00070-08.
[47] X. Zhou, W. Zheng, Y. Li, R. Pearce, C. Zhang, E.W. Bell, et al., I-TASSER-MTD: a deep-learning-based platform for multi-domain protein structure and function prediction, Nat. Protoc. 17 (2022) 2326–2353, https://doi.org/10.1038/s41596-022-00728-0.
[48] J. Saczek, O. Jamieson, J. McClements, A. Dann, R.E. Johnson, A.D. Stokes, et al., Troponin I biomarker sensing from clinical patient samples using molecularly imprinted polymer nanoparticles for advancing healthcare approaches in cardiovascular disease, Biosens. Bioelectron. (2025) 117467, https://doi.org/10.1016/j.bios.2025.117467.
[49] A. Stals, L. Baert, N. Botteldoorn, H. Werbrouck, L. Herman, M. Uyttendaele, et al., Multiplex real-time RT-PCR for simultaneous detection of GI/GII noroviruses and murine norovirus 1, J. Virol. Methods 161 (2009) 247–253, https://doi.org/10.1016/j.jviromet.2009.06.019.
[50] T. Miura, S. Parnaudeau, M. Grodzki, S. Okabe, R.L. Atmar, F.S.L. Guyader, Environmental detection of genogroup I, II, and IV noroviruses by using a generic real-time reverse Transcription-PCR assay, Appl. Environ. Microbiol. 79 (2013) 6585, https://doi.org/10.1128/AEM.02112-13.
[51] G.E. Greening, J. Hewitt, Norovirus detection in shellfish using a rapid, sensitive virus recovery and real-time RT-PCR detection protocol, Food Anal. Methods 1 (2008) 109–118, https://doi.org/10.1007/s12161-008-9018-3.
[52] J. Vinjé, Advances in laboratory methods for detection and typing of norovirus, J. Clin. Microbiol. 53 (2015) 9.
[53] S.R. Ahmed, K. Takemeura, T.-C. Li, N. Kitamoto, T. Tanaka, T. Suzuki, et al., Size-controlled preparation of peroxidase-like graphene-gold nanoparticle hybrids for the visible detection of norovirus-like particles, Biosens. Bioelectron. 87 (2017) 558–565, https://doi.org/10.1016/j.bios.2016.08.101.
[54] A.E.V. Hagström, G. Garvey, A.S. Paterson, S. Dhamane, M. Adhikari, M.K. Estes, et al., Sensitive detection of norovirus using phage nanoparticle reporters in lateral-flow assay, PLoS One 10 (2015) e0126571, https://doi.org/10.1371/journal.pone.0126571.
[55] CerTest BIOTECH, CERTEST Norovirus ONE STEP Norovirus GI and GII CARD TEST, 2016.
[56] L. Hu, W. Salmen, R. Chen, Y. Zhou, F. Neill, J.E. Crowe, et al., Atomic structure of the predominant GII.4 human norovirus capsid reveals novel stability and plasticity, Nat. Commun. 13 (2022) 1241, https://doi.org/10.1038/s41467-022-28757-z.
[57] C. Song, R. Takai-Todaka, M. Miki, K. Haga, A. Fujimoto, R. Ishiyama, et al., Dynamic rotation of the protruding domain enhances the infectivity of norovirus, PLoS Pathog. 16 (2020) e1008619, https://doi.org/10.1371/journal.ppat.1008619.
[58] C. Sun, P. Huang, X. Xu, F.S. Vago, K. Li, T. Klose, et al., The 2.6 Å structure of a tulane virus variant with minor mutations leading to receptor change, Biomolecules 14 (2024) 119, https://doi.org/10.3390/biom14010119.
[59] R. Golmohammadi, K. Valegård, K. Fridborg, L. Liljas, The refined structure of bacteriophage MS2 at 2·8 Å resolution, J. Mol. Biol. 234 (1993) 620–639, https://doi.org/10.1006/jmbi.1993.1616.